



Photoelectrochemical performance of MWCNT–Ag–ZnO ternary hybrid: a study of Ag loading and MWCNT garnishing

Mangesh A. Desai¹, Vidhika Sharma², Mohit Prasad², Girish Gund³, Sandesh Jadkar², and Shrikrishna D. Sartale^{1,*}

¹Thin Films and Nanomaterials Laboratory, Department of Physics, Savitribai Phule Pune University, Pune 411007, India

²School of Energy Studies, Savitribai Phule Pune University, Pune 411007, India

³Department of Physics, M.P.A.S.C. College, Panvel 410206, India

Received: 1 October 2020

Accepted: 16 January 2021

Published online:

8 February 2021

© The Author(s), under exclusive licence to Springer Science+Business Media, LLC part of Springer Nature 2021

ABSTRACT

Herein, by using chemical methods such as successive ionic layer adsorption and reaction (SILAR) and spin coating we have demonstrated a novel strategy for the synthesis of ternary hybrid to study photoelectrochemical (PEC) performance. To the best of our knowledge, for the first time we have represented a case study of achieving optimum SILAR cycles for Ag nanoparticles decoration on ZnO nanorods and a discussion was made on a role of multi-walled carbon nanotube (MWCNT) as a top layer over Ag–ZnO nanostructures for better PEC performance. Firstly, Ag nanoparticles loading over SILAR grown ZnO nanorods was varied for different SILAR cycles to optimize better photocurrent. This Ag–ZnO hybrid showed higher photocurrent density of 0.45 mA/cm² at 1 V bias (vs SCE) and photoconversion efficiency (PCE) of 0.21% (0.45 V vs SCE). Thereafter, MWCNTs were garnished by using spin coating as a top layer on Ag–ZnO hybrid leading to the formation of ternary hybrid of MWCNT–Ag–ZnO for further enhancement of PEC activity. We believe that top layer of MWCNT plays a vital role of electron and hole transfer and bridges Ag decorated ZnO nanorods together leading to well-connected conducting pathways for efficient charge collection and transport. The appropriate band bending of MWCNT–Ag–ZnO hybrid leads to the formation of active interface helping out in charge separation leading to excellent photocurrent density of 0.56 mA/cm² at 1 V bias (vs SCE) and photoconversion efficiency of 0.26% (0.45 V vs SCE).

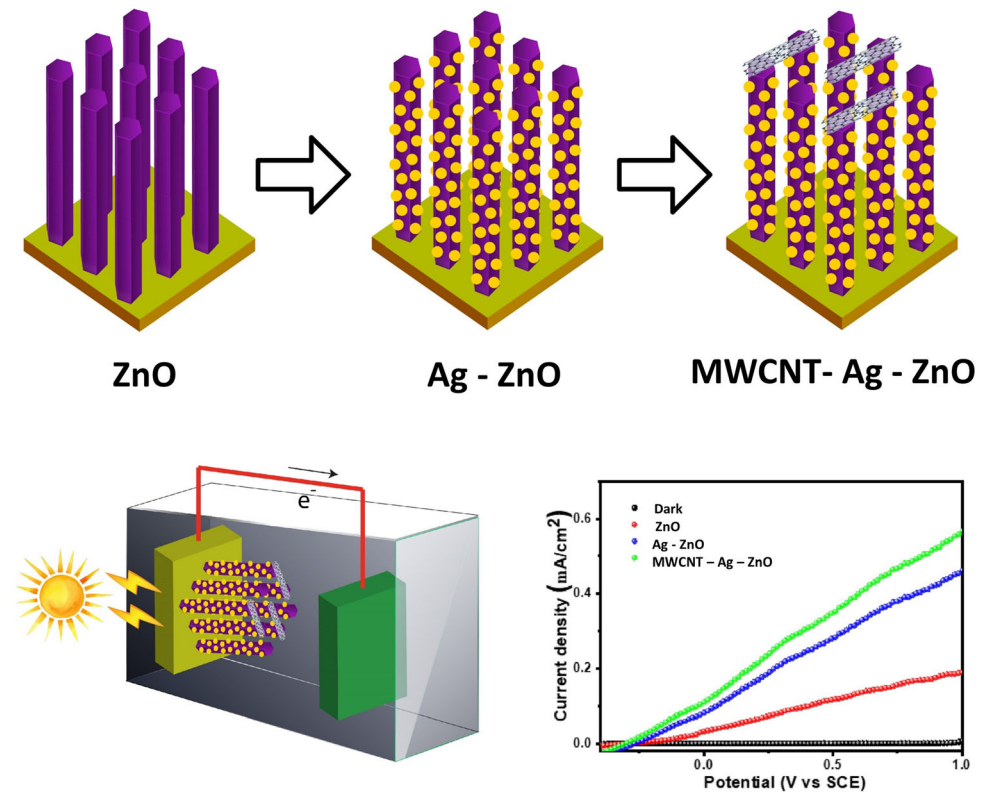
Handling Editor: Kyle Brinkman.

Address correspondence to E-mail: sdsartale@physics.unipune.ac.in

<https://doi.org/10.1007/s10853-021-05821-5>

GRAPHICAL ABSTRACT

Enhanced light harvesting, higher donor density, appropriate band bending, lowest charge transfer radius of C–Ag–ZnO hybrid signifies that efficient charge transfer and restriction to charge recombination leading to the enhanced PEC performance.



Introduction

Tremendous consumption of conventional energy sources causes their fast depletion demanding search of novel ways of energy generation and storage [1, 2]. In the hunt, one of the green energy sources and most promising techniques is water splitting for hydrogen generation with the assistance of sunlight [3]. Since the past few years, several metal oxides such as TiO₂, Fe₂O₃, NiO, BiVO₄ and ZnO are being utilized for efficient water splitting [1, 4]. Among all of them, ZnO is a widely used semiconducting material because of its advantageous properties like high surface area, effective light harvesting, good mobility of electrons, lowest charge transfer resistance, etc. [5].

Such properties can be tuned by molding ZnO into diverse nanostructures like nanopencil, nanorods, nanoflowers, branched nanorods, urchin-like structures, etc. [5–8]. Under light illumination, electrons from the valence band of ZnO get excited to the conduction band. Since reduction and oxidation potentials of water stand exactly within band edge potentials of ZnO leading to an interesting alignment of Fermi levels. This results in faster electronic transport from ZnO to water leading to reduction of water and flow of photocurrent.

However, the band gap of ZnO is 3.37 eV so that it can absorb only ultraviolet (UV) part of electromagnetic spectrum and nearly 97–96% of the solar spectrum remain unabsorbed [5]. Additionally, ZnO has a high recombination rate and charge transfer

resistance limiting the photoelectrochemical (PEC) performance of ZnO. To overcome such drawbacks, it is coupled with other materials to enhance its PEC performance. In the hunt, different strategies were reported to combine ZnO with other materials. Incorporation of dopant in ZnO gives rise to higher light absorption and increment in carrier concentration leading to better conductivity [9]. Owing to surface plasmon resonance of noble metal nanoparticles, their decoration over ZnO can boost visible light harvesting and increase photogenerated charge carrier separation [10]. ZnO is coupled with other visible light active semiconductors like CdS [11], CuO [12], Fe₂O₃ [13], etc. to absorb major part of visible light and better photocurrent. Sensitization of ZnO nanostructures by nanocarbon for finer charge transport and therefore enhanced PEC performance can be achieved [14].

Several previous reports mentioned that Ag decoration and doping in ZnO enhances the photoactivity and photoactivity performance found to be varied with respect to the morphology of ZnO nanostructures, the concentration of Ag precursors, etc. [15–20]. Further increment in PEC performance can be attained by the formation of ternary hybrid (i.e., merging of two such aforementioned strategies). The ternary hybrid structure possesses huge potential in PEC and attracted great attention of scientists due to their astonishing properties like increased absorption of visible light, reduced electron–hole recombination, appropriate band bending for effective charge transfer, improved charge separation and low onset potential. Such various ternary nanocomposites like ZnO/rGO/Ag [21], g-C₃N₄/Pt/ZnO [22], CdS/ZnO/graphene [23], MWCNT/ZnO/GaN [24], CdS/MoS₂/ZnO [25], etc. have been reported in recent years.

It is noteworthy that the incorporation of multi-walled carbon nanotube (MWCNT) over semiconducting photoanode demonstrated significant absorption of visible light, high mechanical and chemical stability and enhanced charge transport due to higher conductivity than semiconductors [14]. Generally, nanocarbon is utilized as the bottom layer (in firm contact with the substrate) and over it other semiconductors are deposited; thus, nanocarbon helps to increase overall conductivity. Sometimes composites of metals or semiconductors are being synthesized with nanocarbon for PEC studies. However, to the best of our knowledge nanocarbon like

MWCNT as a top layer in ternary hybrid and its PEC studies are not reported yet. In this report, we have garnished functionalized MWCNTs over optimized Ag–ZnO hybrid and those MWCNTs form connection between Ag–ZnO nanorods leading to the efficient hole transport resulting in excellent PEC performance.

Successive ionic layer adsorption and reaction (SILAR) is used to synthesize a variety of nanostructures due to its advantages like cost-effectiveness, scalable and feasibility of low temperature deposition on any complex shape substrates, etc. [8, 26]. In our previous report, we have demonstrated seed layer free deposition of ZnO nanorods thin films by using hydrazine hydrate as a source of hydroxyl ions [6]. We concluded that ZnO nanorods deposited for 120 SILAR cycles turn out to be best for PEC performance and selected for present work as hosts for loading of Ag nanoparticles using SILAR method. We have varied SILAR cycles for the deposition of Ag nanoparticles and optimization was done for better PEC performance. MWCNTs were garnished as a top layer over the Ag–ZnO hybrids by using a spin coating method which resulted in superior PEC performance. MWCNTs act as photosensitizer by absorbing light and helps electron and hole transfer. The well-connected conducting pathways of MWCNT are advantageous for efficient charge transport.

Experimental section

MWCNTs, silver nitrate (AgNO₃), zinc nitrate (Zn(NO₃)₂), hydrazine hydrate (N₂H₄·H₂O) and fluorine doped tin oxide (FTO)-coated glass substrate of surface resistivity ~ 10Ω/sq and dimensions of 100 mm × 100 mm × 3 mm were procured from Sigma-Aldrich, India.

SILAR method for deposition of thin films

In contrast to other chemical methods, heterogeneous growth is expected in SILAR method since reactions occur only on the substrate between adsorbed growth species [27]. Generally, the substrate is sequentially immersed in several precursor's solution for certain time, the deposition process is schematically represented in supplementary information Fig S1. The deposition occurs via the following steps.

Step 1 Adsorption: the ions from the precursor solution are adsorbed on substrate and form a liquid layer. Step 2 Rinsing (I): in this step, excess loosely attached or detachable ions are rinsed away from the liquid layer. Step 3 Reaction: the counterions from second precursor solution reacts with pre-adsorbed ions from the first precursor's solution on the substrate to form a thin film on substrate surface. Step 4 Rinsing (II): In the last step, the surplus unreacted species, loosely bound molecules and other reaction byproducts are removed.

ZnO thin film deposition

SILAR deposition of ZnO nanorods thin films is discussed in details in our previous report [6]. In brief, deposition procedure is as follows: Aqueous solutions of 0.01 M $\text{Zn}(\text{NO}_3)_2$ and 0.02 M $\text{N}_2\text{H}_4 \cdot \text{H}_2\text{O}$ were prepared in separate beakers and kept at 75 °C. FTO-coated glass substrate was chosen as substrate and cleaned properly. The clean substrate was immersed successively for 10 s in $\text{Zn}(\text{NO}_3)_2$ and $\text{N}_2\text{H}_4 \cdot \text{H}_2\text{O}$ precursors solutions. Between the immersions, the FTO substrate was also rinsed in double-distilled water (DDW) for 10 s to remove loosely adsorbed species which was also kept at the same temperature as mentioned above. In this way, four successive immersions completed one cycle. Such 120 cycles were performed to deposit well adherent thin films. Furthermore, these thin films were annealed at 350 °C for 4 h in the air atmosphere to improve the crystallinity. All deposition parameters are mentioned in supplementary information Table S1.

Loading of Ag nanoparticles on ZnO thin films

Ag nanoparticles on ZnO nanorods were loaded by SILAR deposition method as reported elsewhere [28]. This deposition was carried out at room temperature. Aqueous solutions of AgNO_3 (0.01 M) and $\text{N}_2\text{H}_4 \cdot \text{H}_2\text{O}$ (0.1 M) were used as precursors. The ZnO nanorod grown FTO substrate was inserted in AgNO_3 solution for 10 s and $\text{N}_2\text{H}_4 \cdot \text{H}_2\text{O}$ solution for 120 s. Meanwhile, it was rinsed in DDW for 15 s after each immersion to remove loosely adsorbed species leading to the completion of one cycle. In this way, 1, 2, 5 and 10 cycles were performed and samples were named as 1-Ag-ZnO, 2-Ag-ZnO, 5-Ag-ZnO and 10-Ag-ZnO,

respectively. All deposition parameters are mentioned in supplementary information Table S1.

Functionalization of MWCNT

MWCNTs were functionalized as per procedure given below. 0.2 g MWCNTs were well dispersed in acidic solution that consists of 5 ml nitric acid (HNO_3) and 15 ml sulfuric acid (H_2SO_4) (3:1 ratio) by using a magnetic stirrer. The solution was kept at 60–80 °C with continuous stirring for 1 h, and the supernatant was separated. Thereafter, it was washed several times with DDW and dried overnight in an oven at 120 °C which gave black-colored powder of functionalized MWCNT.

Garnishing of MWCNT on Ag-ZnO thin films

Among all Ag-ZnO thin films, best PEC performing Ag-ZnO thin film (2-Ag-ZnO) was chosen for the MWCNT garnishing for further enhancement in the photocurrent. 5 mg functionalized MWCNTs were dispersed in 50 ml isopropyl alcohol and ultrasonicated for 4 h to make a well dispersed MWCNTs solution. The garnishing of functionalized MWCNTs was done by using spin coating at 1000 rpm on Ag-ZnO thin films for 5 cycles. The formed hybrid thin films were named as C-Ag-ZnO. We have restricted ourselves up to 5 spin coating cycles because for more than 5 spin cycles MWCNTs were tended to fall down rather than being anchored to the surface of Ag-ZnO thin films due to poor adhesion. Such films were not suitable since electrode material get peeled off during electrochemical studies.

Characterization

X-ray diffraction (XRD) of the hybrid thin films was carried out by using Bruker D8 advance X-ray diffractometer in 2θ range between 20 to 80° with the help of $\text{Cu K}\alpha$ X-ray radiations ($\lambda_{\text{K}\alpha} = 1.5405 \text{ \AA}$). The surface morphology studies were performed under a scanning electron microscope (SEM) JEOL JSM-6360A Japan at 20 kV electron energy and field emission scanning electron microscope (FESEM) Carl Zeiss. Diffuse reflectance spectroscopy (DRS) studies were performed on JASCO V-670 UV-Vis-NIR spectrophotometer by using barium sulfate (BaSO_4) as reference. Raman studies were performed using in

-Via micro-Raman (Renishaw) spectrophotometer with 5% of 60mW power of 532nm laser excitation. X-ray photoelectron spectroscopy (XPS) was performed on PHI Versaprobe III by using Al K α X-rays.

PEC studies

PEC performance of hybrid thin films (working electrode) of area 1 cm² was recorded using a three electrode system, where saturated calomel electrode (SCE) and Pt were used as reference and counter electrodes, respectively, in 0.5 M sodium sulfate (Na₂SO₄) electrolyte solution. PEC studies were performed by focusing simulated light of 150 W from xenon lamp (PEC-L01) of illumination intensity of 100 mW/cm² (AM 1.5) by using potentiostat (Metrohm Autolab PGSTAT302 N) under the variation of applied potential from -0.5 to +1.0 V (vs SCE). For the determination of donor density and flat band potential, Mott-Schottky plots were recorded. Electrochemical impedance studies were carried out in a frequency range of 10⁵–10⁻¹ Hz where AC voltage amplitude was of 5 mV.

Results and discussion

X-ray diffraction (XRD)

Figure 1 shows XRD patterns of ZnO, 1-Ag-ZnO, 2-Ag-ZnO, 5-Ag-ZnO and 10-Ag-ZnO thin films. In accordance with JCPDS card number 361451, all thin films consist of well crystalline zinc oxide with a wurtzite crystal structure. ZnO thin films possess orientations along (10 $\bar{1}$ 0), (0002), (10 $\bar{1}$ 1), (10 $\bar{1}$ 2), (11 $\bar{2}$ 0), (10 $\bar{1}$ 3) and (11 $\bar{2}$ 2) with preferential orientation along (0002) plane. We have plotted intensity in a log scale in the XRD patterns to identify the presence of any impurity; however, no peaks correspond to any impurities, hydroxides or secondary phases were observed. Incidentally, no significant changes in the intensity or peak position of ZnO peaks in the XRD patterns were seen due to Ag decoration. Moreover, after Ag decoration small peak corresponding to (200) plane of FCC Ag crystal structure (JCPDS card number 040783) was emerged and its intensity increased with an increase in decoration of Ag by more SILAR cycles. It is noteworthy that XRD results reveal that Ag is present in the metallic form.

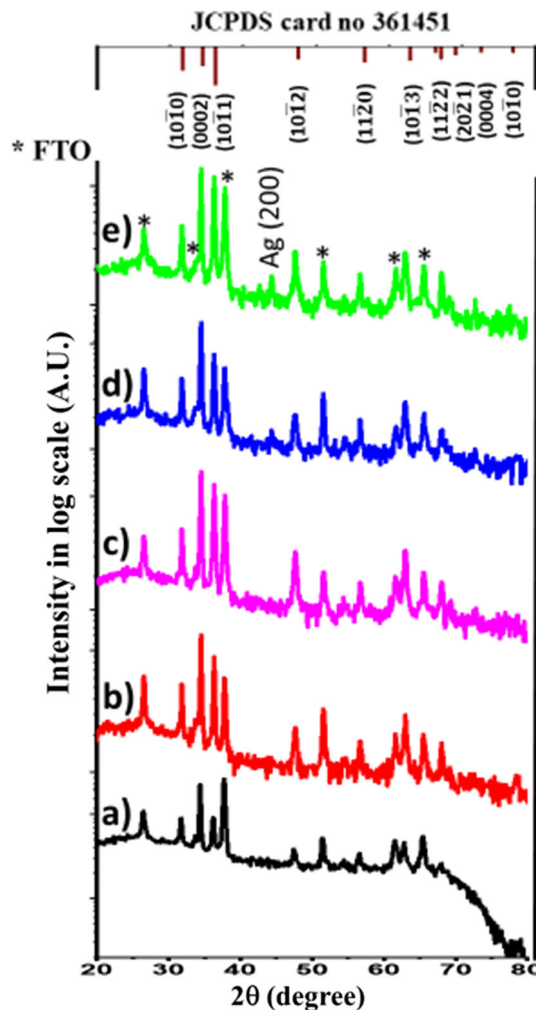
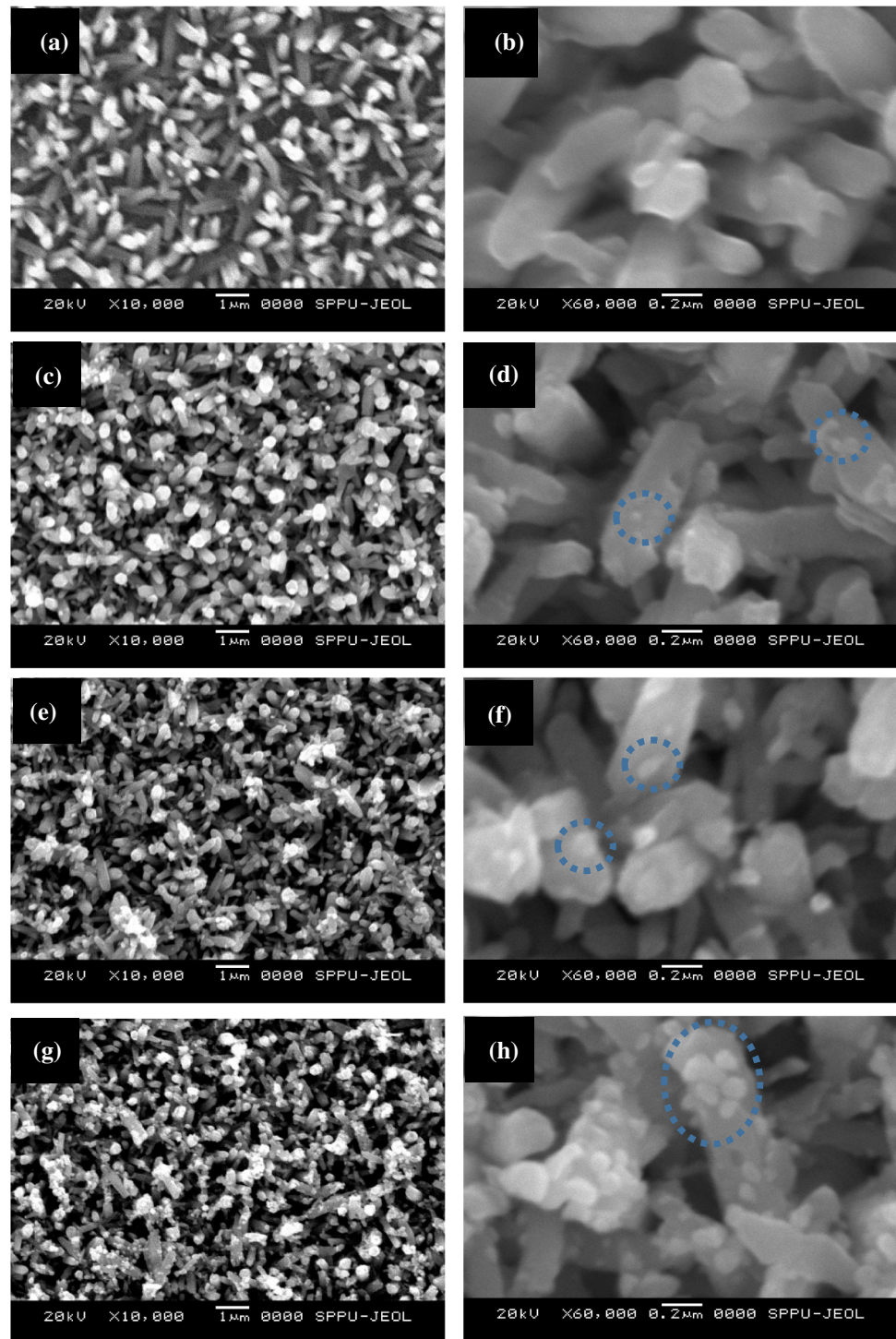


Figure 1 XRD patterns of **a** ZnO, **b** 1-Ag-ZnO, **c** 2-Ag-ZnO, **d** 5-Ag-ZnO and **e** 10-Ag-ZnO thin films. The peaks correspond to FTO-coated glass substrates are denoted by asterisk (*).

Morphological studies

Morphology of the nanostructure is one of the prime aspects for PEC studies because orientation, alignment, shape and size of nanostructures play essential role in the light absorption and establishment of conduction channel for charge carriers. Thus, we have performed detailed study of morphological features of all thin films. Figure 2 illustrates SEM images of ZnO, 1-Ag-ZnO, 2-Ag-ZnO, 5-Ag-ZnO and 10-Ag-ZnO thin films with two different magnifications. Nanorod morphology is clearly evident from all SEM images. As shown in supporting information (Fig S2), pristine ZnO thin film shows a network of nanorods over the entire substrate area without any overgrowth. Figure 2a, b depicts 1-Ag-

Figure 2 SEM images with low (10000X) and high magnification (60000X) s of **a**, **b** 1-Ag-ZnO, **c**, **d** 2-Ag-ZnO, **e**, **f** of 5-Ag-ZnO and **g**, **h** 10-Ag-ZnO thin films.



ZnO thin films consisting of nanorod morphology which are almost similar to the pristine ZnO thin films. Variation in the shape was found for the 2-Ag-ZnO thin films as shown in Fig. 2c, wherein magnified image (Fig. 2d) exhibits growth of few Ag nanoparticles over the ZnO surface shown in circles.

However, for a more detailed understanding of 2-Ag-ZnO thin films we have performed FESEM studies. As seen in FESEM images many rods were found to be grown perpendicular to the substrate whereas few ZnO nanorods were inclined to the substrate (supplementary information Fig S3a).

Magnified FESEM image (supplementary information Fig. S3b) shows the conformal coating of the Ag nanoparticles on the ZnO nanorods wherein many Ag nanoparticles were found in $\sim 20\text{--}30$ nm size range. However, few bigger particles are also grown because of agglomeration of smaller ones. With an increase in the SILAR cycles, the particle size of Ag nanoparticles increases (as seen in SEM images). Accordingly, 5-Ag-ZnO thin film SEM image (Fig. 2e) illustrates oddness in the hexagonal shape with deviation in the perpendicular orientation of ZnO rods and large-sized Ag nanoparticles shown by circles are grown on the ZnO surface (Fig. 2f). The morphology of the 10-Ag-ZnO thin films was found to have most deviated from hexagon-shaped nanorods, and many rods are aligned obliquely to the substrate as shown in Fig. 2g. Moreover, due to the agglomeration of Ag nanoparticles overgrowth (Fig. 2h) was observed leading to the formation of larger-sized particles shown by circles. Variation in the morphology (size and coverage) of Ag nanoparticles on ZnO nanorods is similar to our previous report of Ni nanoparticles [29].

ZnO is amphoteric so that it has tendency to show chemical reactions with high acidic and basic condition. Previously, we observed that variation in concentration of OH^- ions results in a significant change in the morphology and the crystal orientation of ZnO nanostructures [30]. Similarly, preceding reports suggest that higher time or pH exposure (even slight change) to ZnO nanostructures gives rise to variation in their crystal orientation and morphology [31–33]. As compared to the pristine ZnO nanorod deposition, decoration of Ag nanoparticles over ZnO was done with a higher concentration of hydrazine hydrate solution (i.e., 5 times higher concentration of OH^- ions) and substrate was also immersed for a prolonged time (i.e., 12 times higher time) in hydrazine hydrate solution. Therefore, we believe that higher concentration and immersion time of hydrazine hydrate bring out slight variation in crystal orientation, alignment and morphology as we have seen in XRD patterns and SEM images.

Diffused reflectance spectra (DRS) studies

To identify exact band edge positions and study absorption range of thin film DRS is considered to be a vital tool. DRS were recorded from 350 to 800 nm for all thin films as demonstrated in Fig. 3 where a

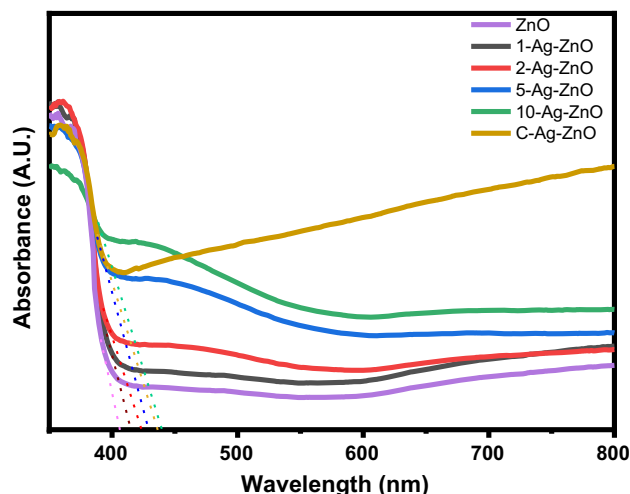


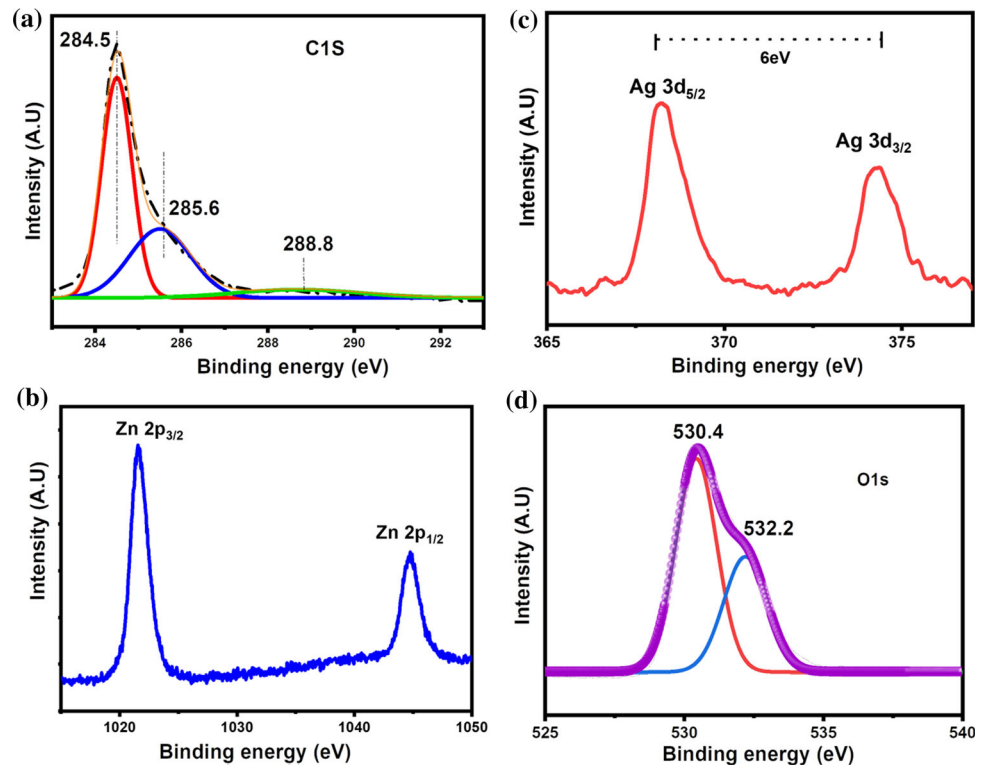
Figure 3 DRS of ZnO, 1-Ag-ZnO, 2-Ag-ZnO, 5-Ag-ZnO and 10-Ag-ZnO thin films.

distinct variation in light absorption was observed for each film. Pure ZnO thin film revealed sharp absorption at ~ 370 nm which can be allocated to the intrinsic band gap of ZnO. It is well known that Ag nanoparticles give rise to absorption of visible light due to localized surface plasmons resonance (LSPR) phenomenon; consequently, all Ag-loaded samples show absorption around 430 to 450 nm [28]. Moreover, with the increase in SILAR cycles absorption due to LSPR was found to be amplified because of increment in Ag nanoparticle decoration. Moreover, band edges slightly shifted toward higher wavelength with an increase in Ag nanoparticle decoration as shown by dotted lines which is in accordance with previous studies [34]. C-Ag-ZnO thin films demonstrated superior light absorption as compared to all films owing to synergetic effect of multiple light scattering centers of MWCNTs and their visible light absorption, Ag nanoparticles and UV absorption capable ZnO nanorods. Such light harvesting considered to be effective for the production of electron hole pairs leading to huge enhancement in the photocurrent [24].

X-ray photoelectron spectroscopy (XPS)

XPS studies were performed to recognize the oxidation states and elemental constituents of C-Ag-ZnO hybrid thin films. Survey spectrum is demonstrated in supporting information Fig S4. The scanned sample comprised of C, Zn, O and Ag, and no impurities were found in the survey spectrum. Figure 4(a–c)

Figure 4 XPS core spectra of **a** carbon (C1s) **b** zinc (Zn2p) **c** silver (Ag3d) and **d** oxygen (O1s) elements of C–Ag–ZnO thin films.



shows individual core spectra of C1s, Zn2p, Ag3d and O1s elements, respectively. The intense peak at 284.5 eV is due to sp^2 hybridized carbon atoms as seen in the core C1s spectra (Fig. 4a). The minor intensity peaks at higher binding energies of 285.6 and 288.8 eV correspond to the sp^3 hybridized carbon atoms at the CNT surface due to attachment of functional groups like carboxyl and hydroxyl group [35]. Zn core spectrum (Fig. 4b) demonstrated that two peaks at binding energies of 1021.4 and 1044.6 eV corresponded to spin–orbit doublet of Zn 2p_{3/2} and Zn 2p_{1/2}, respectively. This is indication of 2+ valence of Zn present in ZnO. Similarly, Ag 3d spin–orbit coupling is apparent from Fig. 4 c, where two distinct peaks observed at binding energies 367.5 and 373.5 eV attributed to Ag 3d_{5/2} and Ag 3d_{3/2}, respectively. The 6 eV difference in the binding energy between Ag 3d_{5/2} and Ag 3d_{3/2} confirms the presence of the Ag in the metallic nature over the surface of the ZnO nanorods [36]. We have noticed that as compared to the standard bulk Ag (368.3 for Ag 3d_{5/2} and 374.3 eV for Ag 3d_{3/2}) doublet peaks were shifted to lower binding energy [37]. The significant shift of 0.8 eV in Ag spectrum toward lower binding energy is attributed to electrons transfer from metal Ag to ZnO which leads to the

formation of Ag–ZnO hybrid nanostructure [38]. Incidentally, deconvolution of individual asymmetric spectrum of O1s spectrum revealed two peaks at 530.4 and 532.2 eV as shown in Fig. 4d. The peak at lower binding energy was due to O^{2-} ions bonded with Zn in ZnO crystal structure, whereas oxygen deficiencies or presence of hydroxyl group due to surface defects group was responsible for a peak at higher binding energy [37].

Raman studies

Identification of molecular vibration and chemical structure can be easily done by using Raman spectroscopy; hence, to confirm the formation of C–Ag–ZnO ternary hybrid nanostructures it is a useful technique. Figure 5a demonstrates the Raman spectrum of C–Ag–ZnO thin films. According to the group theory, phonon modes such as $2E_2$, $2E_1$, $2A_1$ and $2B_1$ are Raman active for the wurtzite crystal structure of ZnO [30]. In this work, E_2 (high) mode at 435 cm^{-1} due to non-polar optical phonons represents the characteristic peak of the wurtzite crystal structure of ZnO, whereas another peak at 332 cm^{-1} aroused due to $2E_2$ mode. A hump at 580 cm^{-1} of $E_1(\text{LO})$ attributed to the defects formation like oxygen

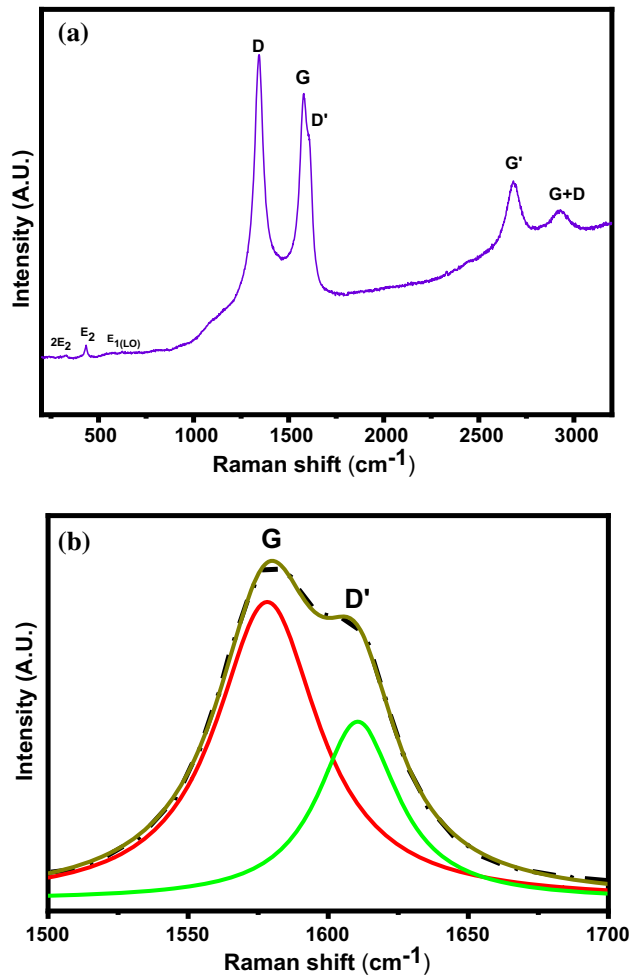


Figure 5 a Raman spectrum and b deconvolution of asymmetric broadening of G band of C–Ag–ZnO thin films.

vacancies and zinc interstitials in the ZnO. Moreover, peaks at higher Raman shift aroused due to MWCNT decoration over ZnO corresponds D, G, D', G' and (G + D) bands. The peak at 1344 cm⁻¹ of D band arises due to the presence of defects and disorder triggered by sp³ hybridization, whereas G band peak at 1576 cm⁻¹ attributed to the planar configuration of the sp² hybridized carbon structure [39]. The higher intensity of Raman peaks of D band than G band (i.e., evolution in the ratio I_D/I_G) proved that some disorder or defect has announced to MWCNT because of their structural modifications by sidewall functionalization and Ag nanoparticles interaction [40]. To understand asymmetric broadening of G band, Lorentzian fitting was performed (Fig. 5b) and two peaks were fitted. The first peak at 1576 cm⁻¹ corresponds to the G band, whereas the second peak at 1640 cm⁻¹ is ascribed to D' band. The past report displayed that

the presence of heteroatom like Ag on CNT was the reason behind origin of D' band [40, 41]. The G' or 2D is second-order band at 2686 cm⁻¹ which is an overtone of D and peak at 2930 cm⁻¹ attributed to the (G + D) band. Overall, the presence of characteristic Raman modes of ZnO and CNT and broadening in G band represents interfacial interaction between C–Ag–ZnO hybrid structures.

ZnO nanorods are totally covered by the Ag nanoparticles; therefore, direct contact between MWCNT and ZnO nanorods is prohibited. Similarly, Ag nanoparticles and MWCNT are in firm contact between each other wherein three types of interactions namely covalent bonding, electrostatic interactions and van der Waals forces are plausible. Firstly, ZnO nanorods were loaded with Ag nanoparticles, and afterward, MWCNTs were garnished, so we rule out covalent bonding possibility between Ag nanoparticles and MWCNT because in XPS results Ag 3d peaks shifted toward lower binding energy due to charge transfer between Ag and ZnO. On the other hand, sidewalls of MWCNT are functionalized with functional groups like carboxyl group and hydroxyls group lead to the production of the charged surface. Therefore, we believe that Ag nanoparticles interact with MWCNT electrostatically which reinforces the presence of D' band in the Raman spectra. XPS and Raman spectra support interaction between MWCNT, Ag nanoparticles and ZnO nanorods leading to the confirmation of formation of C–Ag–ZnO hybrid.

PEC performance

Optimization of SILAR cycles

It is well known in SILAR method with change in cycles, diverse morphologies and variation in the shape and sizes of nanostructures can be easily controlled [8, 26, 30]. Similarly, in our previous report we have varied morphologies and sizes of ZnO nanostructure as well as tuning of Ag nanoparticle size was achieved for better performance in corresponding applications [6, 28, 30]. Optimum decoration of Ag nanoparticles with appropriate size over ZnO nanorods is mandatory to bag better PEC performance. In order to fulfill this requirement, we have decorated Ag nanoparticles over ZnO nanorods under variation of SILAR cycle and their

photochemical properties were studied. By considering better photocurrent and photoconversion efficiency, we compared all thin films of Ag–ZnO hybrids. We found where 2-Ag–ZnO thin film showed improved PEC performance among all (supporting information Fig. S5, S6 and S7); thus, 2-Ag–ZnO thin films were selected for further modification. Therefore, MWCNT decoration was performed on 2-Ag–ZnO thin films only and its performance was compared with pristine ZnO and 2-Ag–ZnO thin films.

Figure 6 illustrates linear sweep voltammetry (LSV), i.e., photocurrent density vs sweep voltage plots of ZnO, Ag–ZnO and C–Ag–ZnO thin films under light and dark conditions. During dark conditions, the minor current was observed due to applied potential, whereas under light illumination large enhancement in the current was observed due to generation of electron hole pairs. Moreover, distinct variations in photocurrent were found for all thin films of ZnO, Ag–ZnO and C–Ag–ZnO. The photocurrent values were hiked at each value of bias potential. However, for comparison of all thin films at 1 V SCE bias photocurrent was found to be hiked from 0.19 to 0.45 and to 0.56 mA/cm² for ZnO to Ag–ZnO and to C–Ag–ZnO thin films, respectively. Interestingly, onset potentials were found to be shifted toward negative potentials as shown in Fig. 6. The calculated onset potential were -0.29, -0.27 and -0.24 V vs SCE for ZnO, Ag–ZnO and C–Ag–ZnO thin films, respectively. Such a shift in the onset potential proved superiority in photoactivity of ternary

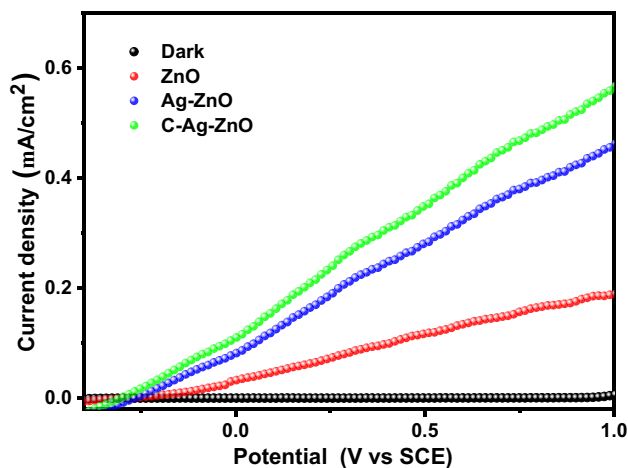


Figure 6 Linear sweep voltammetry (LSV) plots of ZnO, Ag–ZnO and C–Ag–ZnO thin films in 0.5 M Na₂SO₄ solution under light and dark conditions.

photoelectrode of C–Ag–ZnO. The exact mechanism behind improved photocurrent will be discussed in detail in coming section.

It was intriguing to understand more details about donor density and flat band potential of all photoanodes so that further electrochemical studies could be performed. The Mott–Schottky (M–S) plots (i.e., $1/C^2$ vs V) signify several semiconducting properties like flat band potential, type of semiconductor, donor density, etc. All photoanode demonstrated positive slopes as shown in Fig. 7. According to the literature, n-type semiconductor like ZnO demonstrates such kind of behavior [42]. The M–S equation explains the relation between capacitance and electrode potential as follows [21]

$$\frac{1}{C^2} = \frac{2}{e\epsilon\epsilon_0N_d} \left[(V - V_{fb}) - \frac{kT}{e} \right] \quad (1)$$

where e is the charge of the electron, ϵ is the permittivity of ZnO (here we considered it as 10)[43], C is the capacitance of the space charge region, ϵ_0 is the permittivity of the free space, V_{fb} is the flat band potential, $\frac{kT}{e}$ is the temperature dependent term and V is the bias at the electrode material. Moreover, flat band potential (i.e., x-axis intercept) can be calculated by the extrapolation of straight line portion at $1/C^2 = 0$ in M–S plot. All SILAR grown thin films showed a positive shift in flat band potential and the determined flat band potential values were -0.29, and -0.27 and -0.22 V vs SCE for ZnO, Ag–ZnO and C–Ag–ZnO thin films, respectively. Such positive shift in the flat band potential is considered to be essential

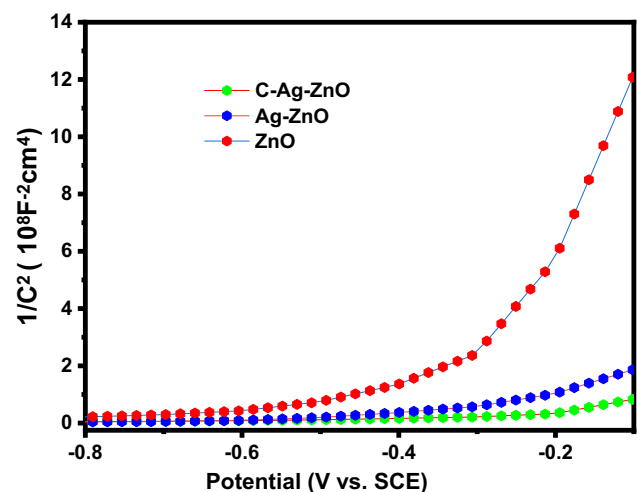


Figure 7 Mott–Schottky (M–S) plots of ZnO, Ag–ZnO and C–Ag–ZnO thin films in 0.5 M Na₂SO₄ solution.

for efficient charge transfer at photoelectrode/electrolyte interface. Positive shift in the flat band potential effectuates an upward lift in valence band leading to the transfer of photoinduced charges and improvement in the oxidizing strength of light-induced holes; thus, finally efficient water oxidation takes place [44, 45].

Furthermore, the slopes determined from M–S plots give an estimation of carrier density (N_d) and it can be calculated as per following formula[6]

$$N_d = \frac{2}{e\epsilon\epsilon_0} \left[\frac{d}{dV} \left(\frac{1}{C^2} \right) \right]^{-1} \quad (2)$$

It is well known that the higher values of carrier densities are beneficial for achieving better PEC performance [6, 44]. The calculated carrier densities were 2.2×10^{21} , 1.99×10^{22} and $3.01 \times 10^{22} \text{ cm}^{-3}$ for ZnO, Ag–ZnO and C–Ag–ZnO thin films, respectively, which are higher than previous reports [46]. As compared to the pristine ZnO films, Ag–ZnO thin films demonstrated an enhancement in carrier density by almost an order of magnitude. This is attributed to the electrons transfer from Ag to ZnO for the alignment of the Fermi levels during charge equilibrium process[44]. Moreover, incorporation of highly conducting MWCNTs further enhances the carrier density in causing synergetic effect of charge transfer at interface of Ag nanoparticles and MWCNTs. Increment in the photocurrent and more negative onset potential are the outcomes of a positive shift in flat band potentials with enhancement in carrier density, thus resulting in the predominant performance of C–Ag–ZnO thin films.

The photoconversion efficiency is the ratio of maximum energy output to the energy supplied in the form of simulated light and can be calculated by the following equation [5]

$$\eta\% = \frac{J_p(E_{rev} - V_{app})}{P_{in}} \times 100 \quad (3)$$

where E_{rev} = standard reversible potential, J_p = measured current density under simulated sun light, P_{in} = incident power density of the illumination of simulated sun light (100 mW/cm^2) and V_{app} = applied bias potential. The maximum photoconversion efficiencies for pristine ZnO photoanode, 2-Ag–ZnO and C–Ag–ZnO were found to be 0.08, 0.21 and 0.26%, respectively, at 0.45 V (vs SCE) as shown in Fig. 8. In short, as compared to the pristine ZnO,

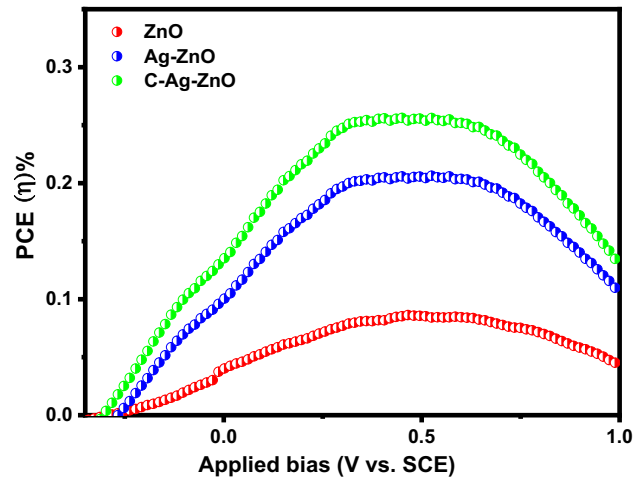


Figure 8 Photoelectrochemical (PEC) efficiency plots against applied bias of ZnO, Ag–ZnO and C–Ag–ZnO thin films.

2-Ag–ZnO photoanode exhibited 2.46 times, whereas C–Ag–ZnO photoanode displayed 3-fold increment in PEC performance.

To understand the charge transfer process at the photoanode/electrolyte interface electrochemical impedance spectroscopy (EIS) is one of the best reliable method. In the Nyquist plot, it is notable that smaller arc radius reflects the effective charge transfer at the photoanode/electrolyte interface. As shown in Fig. 9, the arc radii of photoanodes were related to each other as C–Ag–ZnO < Ag–ZnO < ZnO which indicates pristine ZnO is highly resistive as compared to other films. The decrement in the arc radius was found to be half or less than that in Ag–ZnO and C–Ag–ZnO as compared to the pristine ZnO. As

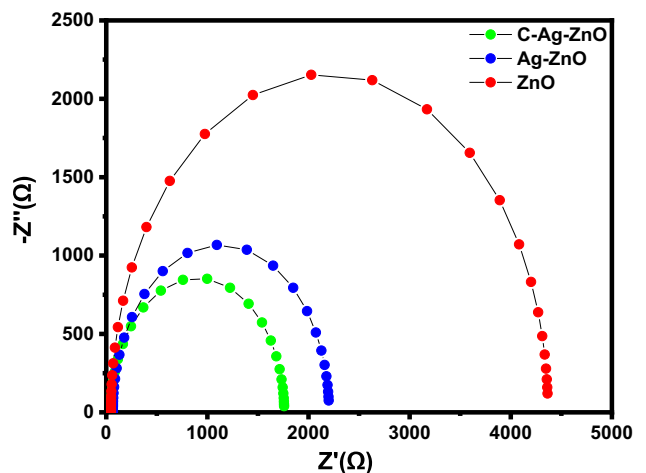


Figure 9 Nyquist plots of ZnO, Ag–ZnO and C–Ag–ZnO thin films.

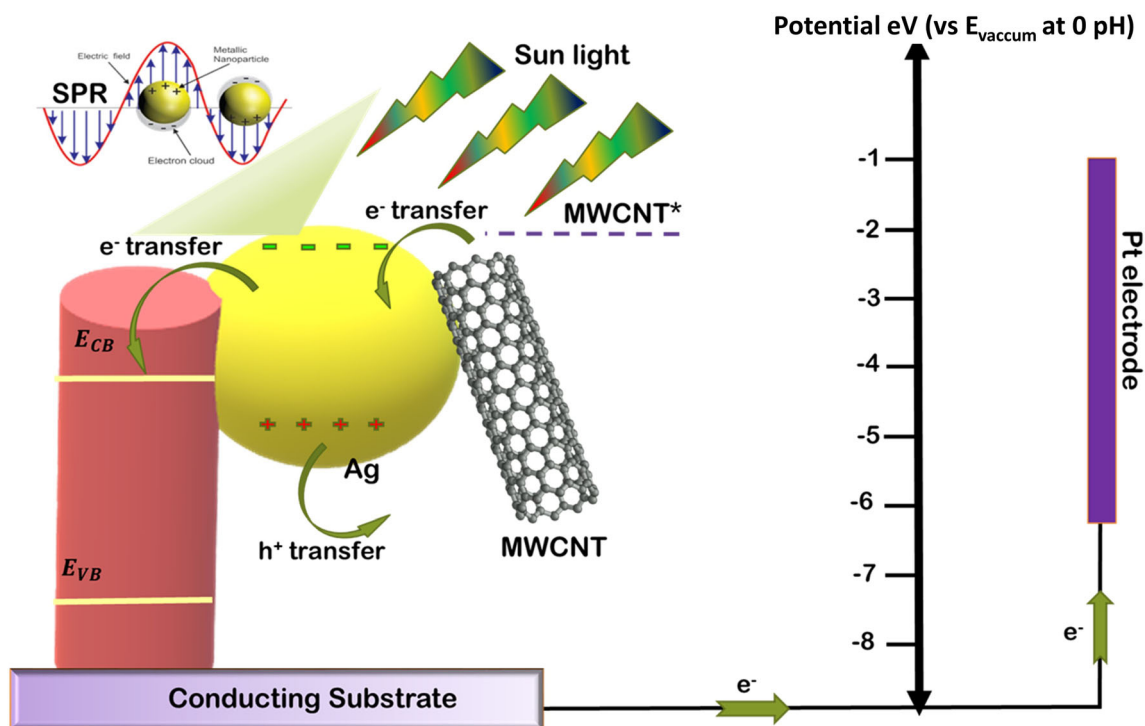


Figure 10 Schematic of PEC mechanism of C–Ag–ZnO thin films.

compared to other thin films, lowest charge transfer radius of C–Ag–ZnO signifies that effective transfer of photogenerated holes at photoelectrode/electrolyte interface due to conductive and dense network of Ag and MWCNT over ZnO leading to enhanced water splitting [45].

Proposed mechanism of PEC performance

As compared to the pristine ZnO thin films, improved PEC performance of C–Ag–ZnO thin films is mainly due to superior light absorption by MWCNTs and LSPR of Ag nanoparticles and higher donor density, appropriate band bending and minimal charge transfer resistance at electrode /electrolyte interface. However, its detail mechanism is given below to understand reasons behind remarkable PEC performance. The decoration of plasmonic Ag nanoparticles over ZnO nanorods causes augmented light absorption and scattering, which aids to the creation of large number of light-induced electron–hole pairs, and additionally, the powerful local electric fields formed in the vicinity of Ag nanoparticles strengthen the segregation of the electron–hole pairs at the interface of Ag–ZnO [47, 48]. In a similar manner, in addition to the LSPR effect of Ag

nanoparticles, garnishing of MWCNT over Ag–ZnO nanorod helps in the increase in the unevenness in hybrid structure which gave rise to increment in light path length due to multiple/high-angle scattering centers leading to efficient light harvesting in C–Ag–ZnO hybrid structure.

On the other hand, previously vertical arrangement of ZnO nanorods was turned out to be supportive for charge electron transfer [6]. Moreover, garnishing of MWCNT forms bridge between many ZnO nanorods which leads to the formation of conducting channel and provides as a network which is favorable for charge collection and transport [49]. Such structural advantage of MWCNTs brings out higher photocurrent and carrier density in C–Ag–ZnO hybrid than Ag–ZnO and pristine ZnO thin films. Moreover, as observed in EIS studies, C–Ag–ZnO hybrid structure offers minimal resistance due to the formation of an active interface between photoelectrode and electrolyte. In addition to that, C–Ag–ZnO hybrid is effective in charge generation, separation and transfer due to phenomenal alignment of band energies whose details are explained below.

It is intriguing to recognize that type of interface formed between different components of nanomaterials due to their band potential energies which

significantly influence light-induced electrons/holes transfer and final PEC activity. The conduction band potential was measured by using the Mulliken electronegativity theory [48, 50].

$$E_{VB} = X + E^\circ + 0.5E_g \quad (4)$$

where X is the absolute electronegativity of the semiconductor and for ZnO it is 5.76 eV (vs NHE), E_g is the band gap energy of the semiconductor, E_{VB} is the valence band edge potential of semiconductor and E° is the energy of free electrons and it is ~ 4.5 eV (vs NHE). Additionally, E_{CB} represents the conduction band edge potential and calculated by the following equation:

$$E_{CB} = E_{VB} - E_g \quad (5)$$

The calculated values of valence band and conduction band potentials were 2.86 eV (vs NHE), i.e., -7.36 eV (vs E_{vacuum}) and -0.34 eV (vs NHE), i.e., -4.16 eV (vs E_{vacuum}) [51]. Moreover, the work functions of Ag and ZnO are 4.3 and 5.2 eV, respectively; thus, the transfer of an electron from Ag to ZnO is favorable [52]. The work function of functionalized MWCNT is 5.1 eV. [53] Moreover, it is proved that MWCNT acts as photosensitizer by absorbing light so that they excited to higher energy level (MWCNT*) leading to electron transfer [54, 55]. Figure 10 demonstrates proposed PEC mechanism of C–Ag–ZnO hybrid structure thin films. The exposure of simulated sun light to MWCNT leads to the formation of an excited state of MWCNT* resulting in electron transfer to Ag nanoparticles. It is proved that strong interaction between Ag nanoparticles and MWCNT rises overall conductivity leading to a boost in total charge carrier concentration as we have observed in carrier density calculations [56]. Meanwhile, upon light exposure, due to LSPR surface plasmon states will be occupied by Ag leading generation of hot electrons. Furthermore, hot electrons get transferred in the conduction band of the ZnO by crossing the Schottky barriers at the Ag–ZnO interface which also helps in restricting electrons from returning to Ag nanoparticles. Moreover, the transfer of an electron to ZnO leaves a hole in Ag nanoparticles. The electrons from the conduction band of ZnO transferred to the Pt counter electrode via conducting substrate and sent to external connection leading to the water reduction with the help of an external potential. On the other hand, holes formed in the Ag nanoparticles supplied to electrolyte solution leading

to oxidation of water. Previously, in PEC photoelectrode hole acceptor mechanism of MWCNTs is also reported [14, 57]. Similar kind of mechanism might be possible in our case also, where MWCNTs may accept holes from Ag nanoparticles and deliver them to the electrolyte solution. To the best of our knowledge, this is the first report wherein top layer garnished MWCNTs electron and hole transporting role in ternary photoelectrode is discussed. In overall, appropriate band alignments in ternary photoelectrode of C–Ag–ZnO amplifies separation of light-induced charges with enhanced electron lifetime and facilitates charge transport leading to improved PEC performance.

Conclusions

We have successfully optimized Ag nanoparticles decoration by varying SILAR cycles over ZnO nanorods for the better PEC performance. Furthermore, on Ag–ZnO hybrid MWCNTs were garnished by using spin coating leading to form ternary hybrid nanostructure of MWCNT–Ag–ZnO verified by the Raman and XPS studies. As compared to the pristine ZnO thin films, 2-Ag–ZnO photoanode exhibited 2.46 times increment in PEC performance whereas MWCNT–Ag–ZnO photoanode displayed 3-fold increment in PEC performance. The MWCNT–Ag–ZnO photoanode exhibited superior light absorption due to the LSPR effect and scattering via multiple reflection centers of morphological architecture. Positive shift in the flat band potential, higher donor density, appropriate band bending and lowest charge transfer radius of MWCNT–Ag–ZnO hybrid signify that effectual charge transfer and restriction to charge recombination lead to the enhanced PEC performance, as compared to the pristine ZnO nanorods thin films.

Acknowledgements

Mangesh A. Desai is thankful to Council of Scientific and Industrial Research (CSIR), India, for awarding senior research fellowship (SRF).

Compliance with ethical standards

Conflict of interest The authors declared that they have no conflict of interest.

Supplementary information: The online version contains supplementary material available at (<http://doi.org/10.1007/s10853-021-05821-5>).

References

- [1] Hisatomi T, Kubota J, Domen K (2014) Recent advances in semiconductors for photocatalytic and photoelectrochemical water splitting. *Chem Soc Rev* 43:7520–7535
- [2] Haladkar SA, Desai MA, Sartale SD, Alegaonkar PS (2018) Assessment of ecologically prepared carbon-nano-spheres for fabrication of flexible and durable supercell devices. *J Mater Chem A* 6:7246–7256
- [3] Li Y, Zhang JZ (2010) Hydrogen generation from photoelectrochemical water splitting based on nanomaterials. *Laser Photonics Rev* 4:517–528
- [4] van de Krol R, Liang Y, Schoonman J (2008) Solar hydrogen production with nanostructured metal oxides. *J Mater Chem* 18:2311–2320
- [5] Desai MA, Vyas AN, Saratale GD, Sartale SD (2019) Zinc oxide superstructures: recent synthesis approaches and application for hydrogen production via photoelectrochemical water splitting. *Int J Hydrog Energy* 44:2091–2127
- [6] Desai MA, Sharma V, Prasad M, Jadkar S, Saratale GD, Sartale SD (2019) Seed-layer-free deposition of well-oriented ZnO nanorods thin films by SILAR and their photoelectrochemical studies. *Int J Hydrog Energy*. <https://doi.org/10.1016/j.ijhydene.2019.09.150>
- [7] Wang T, Lv R, Zhang P, Li C, Gong J (2015) Au nanoparticle sensitized ZnO nanopencil arrays for photoelectrochemical water splitting. *Nanoscale* 7:77–81
- [8] Desai MA, Sartale S (2016) Zinc oxide thin films: nanoflakes to spongy balls via seed layer. *Adv Sci Lett* 22:880–883
- [9] Yang X, Wolcott A, Wang G, Sobo A, Fitzmorris RC, Qian F, Zhang JZ, Li Y (2009) Nitrogen-doped zno nanowire arrays for photoelectrochemical water splitting. *Nano Lett* 9:2331–2336
- [10] Kumari B, Sharma S, Singh N, Verma A, Satsangi VR, Dass S, Shrivastav R (2014) ZnO thin films, surface embedded with biologically derived Ag/Au nanoparticles, for efficient photoelectrochemical splitting of water. *Int J Hydrog Energy* 39:18216–18229
- [11] Li H, Yao C, Meng L, Sun H, Huang J, Gong Q (2013) Photoelectrochemical performance of hydrogenated ZnO/CdS core-shell nanorod arrays. *Electrochim Acta* 108:45–50
- [12] Kargar A, Jing Y, Kim SJ, Riley CT, Pan X, Wang D (2013) ZnO/CuO Heterojunction branched nanowires for photoelectrochemical hydrogen generation. *ACS Nano* 7:11112–11120
- [13] Hsu Y-K, Chen Y-C, Lin Y-G (2015) Novel ZnO/Fe₂O₃ core-shell nanowires for photoelectrochemical water splitting. *ACS Appl Mater Interfaces* 7:14157–14162
- [14] Wei Y, Du H, Kong J, Lu X, Ke L, Sun XW (2014) Multi-walled carbon nanotubes modified zno nanorods: a photoanode for photoelectrochemical cell. *Electrochim Acta* 143:188–195
- [15] Wei Y, Kong J, Yang L, Ke L, Tan HR, Liu H, Huang Y, Sun XW, Lu X, Du H (2013) Polydopamine-assisted decoration of ZnO nanorods with Ag nanoparticles: an improved photoelectrochemical anode. *J Mater Chem A* 1:5045–5052
- [16] Tarwal N, Patil P (2011) Enhanced photoelectrochemical performance of Ag-ZnO thin films synthesized by spray pyrolysis technique. *Electrochim Acta* 56:6510–6516
- [17] Sharma V, Prasad M, Rokade A, Ilaiyaraja P, Sudakar C, Jadkar S (2019) Ag-Au-bimetal incorporated ZnO-nanorods photo-anodes for efficient photoelectrochemical splitting of water. *Energy Technol* 7:233–239
- [18] Thomas M, Sun W, Cui J (2012) Mechanism of Ag doping in ZnO nanowires by electrodeposition: experimental and theoretical insights. *J Phys Chem C* 116:6383–6391
- [19] Lupan O, Cretu V, Postica V, Ahmadi M, Cuenya BR, Chow L, Tiginyanu I, Viana B, Pauporté T, Adelung R (2016) Silver-doped zinc oxide single nanowire multifunctional nanosensor with a significant enhancement in response. *Sens Actuators B Chem* 223:893–903
- [20] Pauporté T, Lupan O, Zhang J, Tugsuz T, Ciofini I, Labat F, Viana B (2015) Low-temperature preparation of Ag-doped ZnO nanowire arrays, DFT study, and application to light-emitting diode. *ACS Appl Mater Interf* 7:11871–11880
- [21] Prasad M, Sharma V, Aher R, Rokade A, Ilaiyaraja P, Sudakar C, Jadkar S (2017) Synergistic effect of Ag plasmon-and reduced graphene oxide-embedded ZnO nanorod-based photoanodes for enhanced photoelectrochemical activity. *J Mater Sci* 52:13572–13585. <https://doi.org/10.1007/s10853-017-1436-4>
- [22] Xiao J, Zhang X, Li Y (2015) A ternary g-C₃N₄/Pt/ZnO photoanode for efficient photoelectrochemical water splitting. *Int J Hydrog Energy* 40:9080–9087
- [23] Han W, Ren L, Qi X, Liu Y, Wei X, Huang Z, Zhong J (2014) Synthesis of CdS/ZnO/graphene composite with high-efficiency photoelectrochemical activities under solar radiation. *Appl Surf Sci* 299:12–18
- [24] Patil SS, Johar MA, Hassan MA, Patil DR, Ryu S-W (2018) Anchoring MWCNTs to 3D honeycomb ZnO/GaN heterostructures to enhancing photoelectrochemical water oxidation. *Appl Catal B* 237:791–801
- [25] Tang Y, Zheng Z, Sun X, Li X, Li L (2019) Ternary CdS-MoS₂ coated ZnO nanobrush photoelectrode for one-

- dimensional acceleration of charge separation upon visible light illumination. *Chem Eng J* 368:448–458
- [26] Desai MA, Sartale SD (2014) ZnS nanoflakes deposition by modified chemical method. *AIP Conf Proc* 1591:1763–1765
- [27] Pathan H, Lokhande C (2004) Deposition of metal chalcogenide thin films by successive ionic layer adsorption and reaction (SILAR) method. *Bull Mater Sci* 27:85–111
- [28] Shaikh IM, Sartale SD (2018) SILAR grown Ag nanoparticles as an efficient large area SERS substrate. *J Raman Spectrosc* 49:1274–1287
- [29] Vyas AN, Desai MA, Phase DM, Saratale RG, Ambekar JD, Kale BB, Pathan HM, Sartale SD (2019) Nickel nanoparticles grown by successive ionic layer adsorption and reaction method for ethanol electrooxidation and electrochemical quartz crystal microbalance study. *New J Chem* 43:2955–2965
- [30] Desai MA, Sartale SD (2015) Facile soft solution route to engineer hierarchical morphologies of ZnO nanostructures. *Cryst Growth Des* 15:4813–4820
- [31] Wahab R, Ansari S, Kim YS, Song M, Shin H-S (2009) The role of pH variation on the growth of zinc oxide nanostructures. *Appl Surf Sci* 255:4891–4896
- [32] Pawar RC, Shaikh JS, Babar AA, Dhare PM, Patil PS (2011) Aqueous chemical growth of ZnO disks, rods, spindles and flowers: pH dependency and photoelectrochemical properties. *Sol Energy* 85:1119–1127
- [33] Rozati SM, Moradi S, Golshahi S, Martins R, Fortunato E (2009) Electrical, structural and optical properties of fluorine-doped zinc oxide thin films: Effect of the solution aging time. *Thin Solid Films* 518:1279–1282
- [34] Varma RS, Thorat N, Fernandes R, Kothari DC, Patel N, Miotello A (2016) Dependence of photocatalysis on charge carrier separation in Ag-doped and decorated TiO₂ nanocomposites. *Catal Sci Technol* 6:8428–8440
- [35] Moraes RA, Matos CF, Castro EG, Schreiner WH, Oliveira MM, Zarbin AJ (2011) The effect of different chemical treatments on the structure and stability of aqueous dispersion of iron-and iron oxide-filled multi-walled carbon nanotubes. *J Braz Chem Soc* 22:2191–2201
- [36] Chen C, Zheng Y, Zhan Y, Lin X, Zheng Q, Wei K (2011) Enhanced Raman scattering and photocatalytic activity of Ag/ZnO heterojunction nanocrystals. *Dalton Trans* 40:9566–9570
- [37] Bazant P, Kuritka I, Munster L, Kalina L (2015) Microwave solvothermal decoration of the cellulose surface by nanostructured hybrid Ag/ZnO particles: a joint XPS XRD and SEM study. *Cellulose* 22:1275–1293
- [38] Zhang X, Wang Y, Hou F, Li H, Yang Y, Zhang X, Yang Y, Wang Y (2017) Effects of Ag loading on structural and photocatalytic properties of flower-like ZnO microspheres. *Appl Surf Sci* 391:476–483
- [39] Sawant SY, Kim JY, Han TH, Ansari SA, Cho MH (2018) Electrochemically active biofilm-assisted biogenic synthesis of an Ag-decorated ZnO@C core-shell ternary plasmonic photocatalyst with enhanced visible-photocatalytic activity. *New J Chem* 42:1995–2005
- [40] Travessa DN, Silva FSd, Cristovan FH, Jorge Jr AM, Cardoso KR (2014) Ag ion decoration for surface modifications of multi-walled carbon nanotubes. *Mater Res* 17:687–693
- [41] Corio P, Santos A, Santos PS, Temperini MLA, Brar V, Pimenta MA, Dresselhaus M (2004) Characterization of single wall carbon nanotubes filled with silver and with chromium compounds. *Chem Phys Lett* 383:475–480
- [42] Allagui A, Alawadhi H, Alkaaby M, Gaidi M, Mostafa K, Abdulaziz Y (2016) Mott-Schottky analysis of flower-like ZnO microstructures with constant phase element behavior. *Physica Status Solidi (a)* 213:139–145
- [43] Yang Y, Guo W, Wang X, Wang Z, Qi J, Zhang Y (2012) Size dependence of dielectric constant in a single pencil-like ZnO nanowire. *Nano Lett* 12:1919–1922
- [44] Chaudhary D, Singh S, Vankar VD, Khare N (2017) A ternary Ag/TiO₂/CNT photoanode for efficient photoelectrochemical water splitting under visible light irradiation. *Int J Hydrog Energy* 42:7826–7835
- [45] Chiu Y-H, Chang K-D, Hsu Y-J (2018) Plasmon-mediated charge dynamics and photoactivity enhancement for Au-decorated ZnO nanocrystals. *J Mater Chem A* 6:4286–4296
- [46] Rokade A, Rondiya S, Sharma V, Prasad M, Pathan H, Jadkar S (2017) Electrochemical synthesis of 1D ZnO nanoarchitectures and their role in efficient photoelectrochemical splitting of water. *J Solid State Electrochem* 21:2639–2648
- [47] Trang TNQ, Phan TB, Nam ND, Thu VTH (2020) In Situ charge transfer at the Ag@ZnO photoelectrochemical interface toward the high photocatalytic performance of H₂ evolution and RhB degradation. *ACS Appl Mater Interf* 12:12195–12206
- [48] Adam RE, Pirhashemi M, Elhag S, Liu X, Habibi-Yangjeh A, Willander M, Nur O (2019) ZnO/Ag/Ag₂WO₄ photoelectrodes with plasmonic behavior for enhanced photoelectrochemical water oxidation. *RSC Adv* 9:8271–8279
- [49] Shu Q, Wei J, Wang K, Zhu H, Li Z, Jia Y, Gui X, Guo N, Li X, Ma C (2009) Hybrid heterojunction and photoelectrochemistry solar cell based on silicon nanowires and double-walled carbon nanotubes. *Nano Lett* 9:4338–4342
- [50] Pirhashemi M, Habibi-Yangjeh A (2017) Ultrasonic-assisted preparation of plasmonic ZnO/Ag/Ag₂WO₄ nanocomposites with high visible-light photocatalytic performance for

- degradation of organic pollutants. *J Colloid Interf Sci* 491:216–229
- [51] Zhang H, Chen G, Bahnemann DW (2009) Photoelectrocatalytic materials for environmental applications. *J Mater Chem* 19:5089–5121
- [52] Wu Z, Xu C, Wu Y, Yu H, Tao Y, Wan H, Gao F (2013) ZnO nanorods/Ag nanoparticles heterostructures with tunable Ag contents: a facile solution-phase synthesis and applications in photocatalysis. *CrystEngComm* 15:5994–6002
- [53] Ago H, Kugler T, Cacialli F, Salaneck WR, Shaffer MS, Windle AH, Friend RH (1999) Work functions and surface functional groups of multiwall carbon nanotubes. *J Phys Chem B* 103:8116–8121
- [54] Oh W-C, Zhang F-J, Chen M-L (2010) Characterization and photodegradation characteristics of organic dye for Pt–titania combined multi-walled carbon nanotube composite catalysts. *J Ind Eng Chem* 16:321–326
- [55] Oh W-C, Chen M-L (2008) Synthesis and characterization of CNT/TiO₂ composites thermally derived from MWCNT and titanium (IV) n-butoxide. *Bull Korean Chem Soc* 29:159–164
- [56] Zhao Q, Tan S, Xie M, Liu Y, Yi J (2018) A study on the CNTs-Ag composites prepared based on spark plasma sintering and improved electroless plating assisted by ultrasonic spray atomization. *J Alloy Compd* 737:31–38
- [57] Lan F, Li G (2013) Direct observation of hole transfer from semiconducting polymer to carbon nanotubes. *Nano Lett* 13:2086–2091

Publisher's Note Springer Nature remains neutral with regard to jurisdictional claims in published maps and institutional affiliations.